Experimental Thermal and Fluid Science 35 (2011) 1184–1192

Contents lists available at ScienceDirect

Experimental Thermal and Fluid Science

journal homepage: www.elsevier.com/locate/etfs

# Characterization of patterns in rimming flow

R. Chicharro [a,*], A. Vazquez [a], R. Manasseh [b,c,d]

[a] Universidad Nacional Autónoma de México – Facultad de Ciencias, Laboratorio de Fluidos, Av. Universidad 3000, Delegación Coyoacán C.P. 04510, México D.F, Mexico
[b] Faculty of Engineering & Industrial Sciences, Swinburne University of Technology, Hawthorn, VIC 3122, Melbourne, Australia
[c] Department of Mechanical Engineering, University of Melbourne, VIC 3010, Melbourne, Australia
[d] Fluid Dynamics Group, CSIRO Materials Science and Engineering, PO Box 56, Highett, VIC 3190, Melbourne, Australia

ARTICLE INFO

*Article history:*
Received 17 December 2010
Received in revised form 12 April 2011
Accepted 13 April 2011
Available online 22 April 2011

*Keywords:*
Axial perturbation
Coating flow
Fast Fourier transform
Recurrence map
Rimming flow
Thin film

ABSTRACT

Patterns were generated inside a horizontal cylinder rotating at low speeds. The cylinder was filled with a very low volume liquid fraction of 1.8% of Newtonian fluid and the rotation speed ranged between 0.08 and 5.2 $s^{-1}$. A novel laser-plane technique was utilized to obtain time series from each pattern. This enabled the characterization of fluid patterns using Fourier spectral (*FS*) and dynamical-systems (chaotic) techniques such as the recurrence map, correlation dimension ($D_2$) and Hurst exponent ($H$). Four patterns were found (fingers, furrows, waterfall and smooth tooth) before annular flow was reached. The results indicate that the *FS* technique not is suitable for flow pattern characterization; and $H$ only has the ability to indicate a possible pattern change. The best tool for indicating the pattern transitions and the inner coat liquid evolution was found to be recurrence maps and $D_2$.



## 1. Introduction

The evolution of a thin liquid coating on or inside a right circular cylinder that is undergoing rotation about a horizontal axis is called rimming flow [1]. A cylinder undergoing uniform rotation is able to hold a thin coating of liquid, due to the combined effects of liquid viscosity and cylinder rotation. In general, however, the coating on a long right circular cylinder may be subject to instability due to the action of surface tension at the liquid–air interface and centripetal acceleration [2]. The analysis of this problem requires an understanding of the interplay between gravitational, rotational and surface tension effects on the coating.

This type of flow has many industrial applications: in the paper industry (the Fourdrinier machine), the roller-coating industry (photographic films, aluminum foils), and in liquid degassers, liquid cooling of turbine shafts, etc. Further numerous topics in applied engineering science are noted by Karapantsios et al. [3], Benkreira et al. [4], and Wilhelmsson et al. [5]. In industry the low liquid volume fractions (1–5%) are very important, especially in the pharmaceutical industry in which the coating provides a sustained release barrier for drug transport. In these systems the coating variability has a strong dependency on surface velocity of a rotating drum, and recent studies reveled that a uniform flow is reached for high rotation speeds Sandadi et al. [6]. In the present paper, we focus on the flow patterns observed at low liquid volume fraction and using a Newtonian fluid. In this regime, Vallette et al. [7] realized experiments using a glass cylinder of radius $R_0 = 5$ cm, length $L = 50$ cm and partially filled with silicone oil ($\mu = 10$ cS) using filling fractions of $A = 1$–4% (where $A = 100V_L/V_T$, with $V_L$,$V_T$ being the fluid and cylinder volume respectively). They investigated the bifurcations to time-dependent and chaotic one-dimensional fluid fronts inside the horizontal rotating tube. A primary cellular pattern undergoes a variety of secondary transitions, depending on the filling fraction. Chen et al. [8] indicated that no information was available for rimming flow for liquid volume fractions less than 2%, despite its industrial importance. Chen et al. [8] used Newtonian solutions of glycerol and polyvinyl alcohol (PVA) of low viscosity (28.4–4.8 cP) and observed the existence a certain critical volume fraction ($V_C$) for each solution, where the rotational speed required to achieve uniform rimming flow takes a minimum value. For $V > V_C$ the patterns are mainly the "shark-tooth" and turbulent regimes, while for $V < V_C$, "fingers" and "rings" are formed. In addition, they found a critical rotational speed ($\Omega_c$) for the annular flow to exist; for water this is $\approx 6$ $s^{-1}$ with a filling fraction $\approx 2\%$, and for $A < 0.5\%$ the rotation speed for annular flow to exist is inversely proportional to the volume fraction.

Numerical and experimental work was realized by Evans [9] in who presented three-dimensional numerical simulations for filling fraction of $\sim 1.9\%$ and silicone oil with $\mu = 48$ cP. The liquid motion was described using a lubrication model and the results exhibit similar fingering to that observed in laboratory experiments for

* Corresponding author.
*E-mail address:* RMANASSEH@groupwise.swin.edu.au (R. Chicharro).

0894-1777/$ - see front matter © 2011 Elsevier Inc. All rights reserved.
doi:10.1016/j.expthermflusci.2011.04.005

**Nomenclature**

| | | | |
|---|---|---|---|
| $A$ | filling fraction (%) | $V_C$ | critical volume fraction ($m^3$) |
| $h$ | coating thickness (m) | $V_L$ | liquid volume ($m^3$) |
| $d$ | embedding dimension (dimensionless) | $V_T$ | cylinder volume ($m^3$) |
| $D_2$ | correlation dimension (dimensionless) | $\mu$ | coating viscosity (cP) |
| $f$ | frequency (Hz) | $\sigma$ | surface tension ($Nm^{-1}$) |
| $H$ | Hurst $t$ exponent (dimensionless) | $\tau$ | time delay (dimensionless) |
| $L$ | cylinder length (m) | $\Omega$ | cylinder rotation rate ($s^{-1}$) |
| $R_0$ | cylinder radius (m) | | |

rotation rate $<2\pi\ s^{-1}$. Investigations for Newtonian and non-Newtonian fluids were carried out by Johnson [10,11] beginning from the lubrication approximations of the hydrodynamic equations, and he was able to demonstrate the presence of a recirculating zone and several possible flow configurations, but could not provide predictions for the transitions to these solutions. Meanwhile Melo [12] investigated experimentally the applicability of the lubrication approximation to the flow in the low fluid volume limit.

When a wider variety of cases than the present low-volume fraction regime are considered, there have been many studies in the literature [13–15]. As noted below, they show the richness of rimming flow with respect to rotation speed, various filling fractions and fluid phase used.

The study of rimming flow began with the experimental work of Balmer [16] who observed the presence of "hygrocysts" in the internal walls of the tube. Later, other authors indicated the existence of large axial variations in coating "bands", finding that the number of bands per unit cylinder length increased approximately linearly with the cylinder rotation rate [17,18]. Chicharro [19] developed a phase diagram in which the "basic" (stagnant) and wavy flow patterns are indicated for low rotation rate using glycerol as the fluid.

Thoroddsen and Mahadevan [20] observed the formation of "shark teeth" along the cylinder axis, in which the spacing between the teeth depends on the rotation speed of the cylinder. Boote and Thomas [21] added small granules (solid spherical glass beads) to the liquid and they observed transitions between various types of structures such as thicker bands (high particle loadings) separated by thin almost-particle-free regions. The previous pattern is very similar to the banding phenomena developing inside horizontal, partially fluid-filled Taylor–Couette systems containing granular additives [22].

It is important to not only observe the rimming flow but to obtain a characterization of the phenomena. In this sense, the first theoretical flow-pattern characterization was obtained by Moffatt [23] who derived an equation for predict the coating thickness $h = V_L/2\pi R_0 L$ for rimming flow outside or inside a rotating horizontal cylinder at low Reynolds numbers. He proposed a minimum rotation speed ($\Omega_c$) at which an annular flow pattern would be reached; here the fluid and cylinder are rotating together as a solid of revolution. In this case, Moffatt [23] established that the Stokes number ($St = \rho g h^2/\mu\,\Omega_c\,R_0$), in which $\rho$ is the fluid density; the Stokes number represents the ratio of gravitational to viscous forces, and had a value of $St \approx 3.14$ when the annular pattern occurs. This prediction was confirmed for a film-dragging experiment by Melo [12].

Preziosi and Joseph [24] introduced a dimensionless number $J = \rho w_c^2 (R_0 - h)^3/\sigma$, indicating the ratio of fluid inertia to surface tension. They found that the annular flow pattern could occur only if $J > 4$. Fomin [25] found three regimes in the rimming flow of non-Newtonian fluid using a scale analysis and non-dimensional parameters. He identified the subcritical (fluid film thickness is a continuous), critical (corner on the rising wall) and supercritical (hydraulic jump) regimes, which depend on a critical mass flux ($q_{max}$).

Rimming flow is analogous to many other physical phenomena in which variations in a parameter control the regime selected. In just one example, bubbling flows, the bubble generation rate (also called the bubbling or sparging rate) determines the kind of flow regime in the system [26]. To characterize such regimes several techniques are used, such as the Fourier spectral (*FS*) and chaotic time series analysis [27–30]. In the present paper, we apply the above methodologies to rimming flow phenomena.

It is clear that the flow patterns in rimming flow are strongly influenced by the liquid volume fraction, fluid surface tension, viscosity and cylinder rotation rate, while, of course, maintaining the same geometrical system parameters ($R_0$, $L$). The aim of the present study is the experimental determination of the pattern transitions for a low filling fraction of 1.8%, using distilled water and with cylinder rotation rate of 0.05–5.2 $s^{-1}$, and their analysis by dynamical-systems tools.

## 2. Experimental set-up

### 2.1. Pattern visualization

A sketch of the experimental system is shown in Fig. 1. The right-circular Plexiglass cylinder has a radius and length of 4.7 cm and 67 cm respectively, and is held at both flat ends with two mobile supports. The left mobile support is attached to a rigid arm while the right is attached to a servo-motor mechanism. The servo-motor (Reliance Electric Model E19–3, Reliance Motion Control Inc., Gallipolis OH, USA) is connected to a servo-motion programmable controller card (Galil Motion Control Inc., Palo Alto CA, USA) which is able to control rotation rates of 0.04–122 $s^{-1}$. The rotation rate was measured with a handheld digital laser tachometer (DT-209X-S12, Nidec-Shimpo Corp., USA). Finally the interface card is connected to a PC (Gateway Inc., Irvine CA, USA).

The filling fraction was 1.8% (70.7 ml, measured with a pycnometer) and the liquid used was distilled water with $\mu = 1$ cP taken from tables. For the visualization patterns a 300 W incandescent light bulb (located at 80 cm distance from the cylinder) was utilized in shadowgraph mode: the front side of the cylinder was illuminated and the back-light was collected on a non-reflective white screen, where the two-dimensional projection of the flow pattern was observed. The patterns were recorded with a high speed color camera Olympus i-SPEED (Olympus KeyMed, Ltd., United Kingdom) at 500 frames for second with a resolution of 800 × 600 at 8 bit.

### 2.2. Pattern characterization

The appearance of patterns as a function of $\Omega$ are only qualitative information. The patterns were generated at the cylinder rear-face, where the liquid rose owing to the clockwise rotation of tube

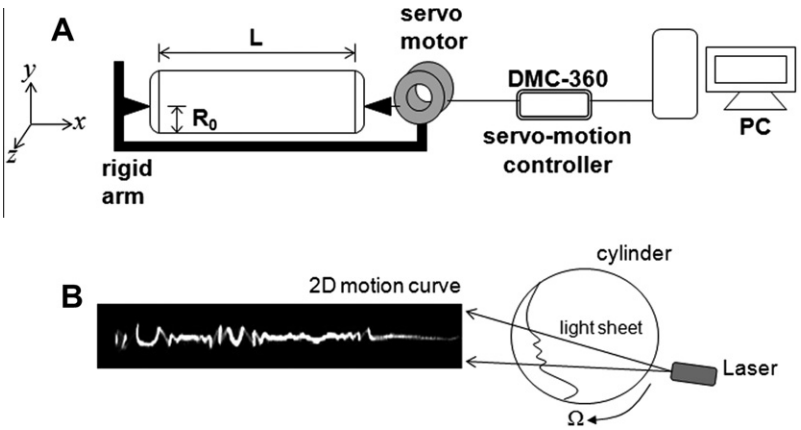


**Fig. 1.** (A) General description of rotating-experimental set-up and (B) the light curve is the instantaneous free surface projection.

and at the free surface of the liquid–air interphase, and are really 3D patterns. The figures III–V are the result of a 2D light-projection (shadowgraph) while figures I, II, VI, VII are direct photographs of the system and they indicate the flow of the free surface.

In order to obtain quantitative information with which to characterize these patterns, a laser beam (Shanghai Dream Lasers Technology Co., Ltd, China) of 532 nm at 500 mW was directed via a cylindrical lens to obtain a light sheet which was sent onto the long horizontal cylinder (Fig 1B). The output of light sheet was collected on a dark non-reflective screen yielding a 2D motion curve or time series. This measurement could be described mathematically as a reduction of the degrees of dimensionality of the system (a projection) and is utilized in mathematical applied sciences when the original phenomena are very complex [31,32], although in our case is the first time that it is used for rimming flow phenomena. We believe that this is a first step to obtain quantitative data and subsequently to apply the Fourier spectral and chaotic methods for the characterization of the patterns. The 2D motion curve was captured as a binary image then converted to data points using ImageJ V-1.40f (Rasband, 1997–2008). The experimental data can then be plotted with any usual graphing software.

## 3. Flow patterns and phase diagram

The rotation speed was varied in the 0–5.2 $s^{-1}$ range in steps of 0.04 $s^{-1}$. When $\Omega = 0$ the fluid is stagnant at the bottom of the cylinder and this is called the "pool" (Fig. 2I). When the speed is increased to $\Omega < 0.08\ s^{-1}$, the fluid continues to show a straight contact line and is describes as a general circular flow ("basic flow"), which has symmetry along the $x$-axis and continues to be located at the bottom of cylinder (Fig. 2II). When $\Omega$ is between

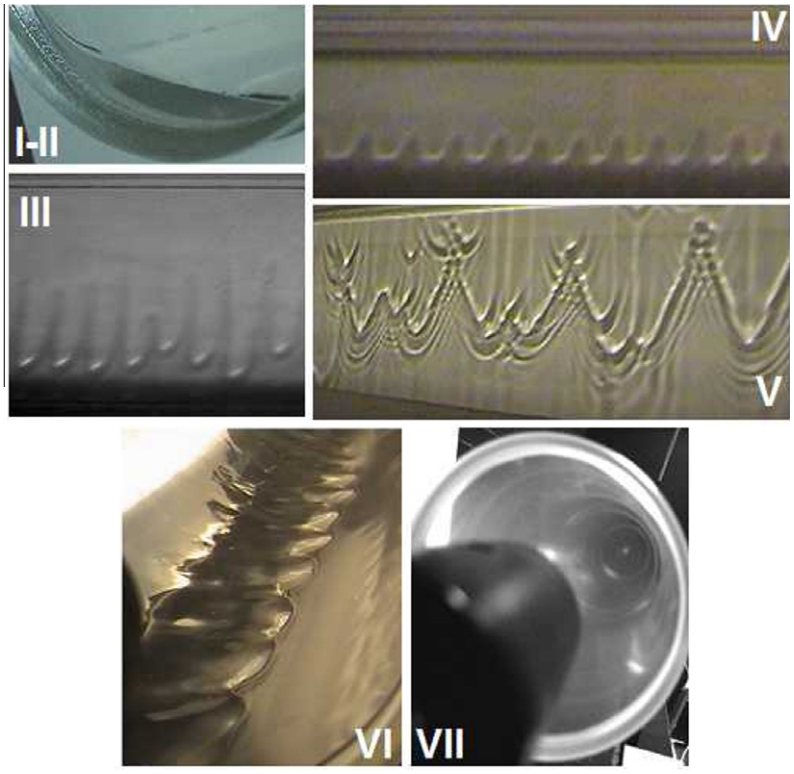


**Fig. 2.** Patterns observed in the horizontal tube, (I) pool, (II) basic, (III) fingers, (IV) furrows, (V) waterfall, (VI) smooth tooth and (VII) annular flow.

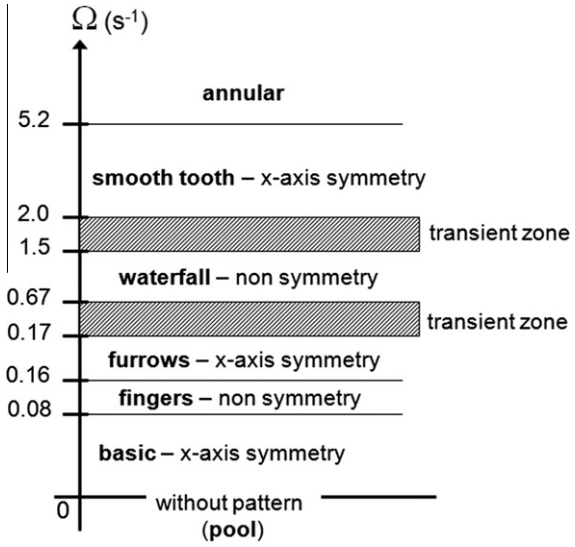


**Fig. 3.** Phase diagram for the rimming flow with a filling fraction of 1.8%.

0.08–0.16 $s^{-1}$ the "fingers" pattern is observed (Fig. 2III); the fingers are located on the wall on which the in the liquid is rising. In this pattern, the fingers vary in size in the *x*-direction. When the rotation speed is above $\Omega = 0.16\ s^{-1}$ a "furrows" pattern is identified (Fig. 2IV) and persists in the 0.16–0.17 $s^{-1}$ interval; in this regime *x*-axis symmetry is again attained. A transient zone is reached when $\Omega = 0.17\ s^{-1}$ in which no pattern is observed. At $\Omega = 0.67\ s^{-1}$ the "waterfall" pattern is observed (Fig. 2V), in which the axial symmetry is absent and the pattern persists in the 0.67–1.5 $s^{-1}$ range; at the end of this interval a new transient zone is identified and again no pattern is observed. The "smooth tooth" pattern is reached when $\Omega = 2.0\ s^{-1}$ (Fig. 2VI). In this pattern, the axial symmetry is regained, with fluid located at the bottom of cylinder. Finally, the last pattern is identified when $\Omega = 5.2\ s^{-1}$ (Fig. 2VII) in which the fluid and cylinder are rotating together (as "a solid of revolution" or "annular flow"). Based on the observations above, a phase diagram can be created, and is shown in Fig. 3.

## 4. Fourier spectral and dynamical-systems (chaotic) time series analysis

### 4.1. Fourier spectral (FS)

A full description of the *FS* and other methods below was given by Vazquez [33]. The *FS* method is frequently used to characterize flow regimes in fluid dynamics. With this tool a preliminary identification of dynamic changes of the rimming flow regimes is possible, and perhaps other analysis tools are needed to further identify and explain the complex behavior. In the case of rimming flows, some researches have fully characterized transitions in the evolution of a one-dimensional fluid front inside a horizontal rotating cylinder, using space–time spectral, correlation analysis, and complex demodulation methods [32]. In the present work the *FS* method is realized by the OriginPro v8.0724 package using a Welch (Gaussian) window with a FFT size of 65536 points.

### 4.2. Hurst exponent (H)

Hurst analysis has been used to study hydrodynamics of three-phase and two-phase fluidized beds [31], trickle beds [34], bubble columns [35], flowing sand [36,37] and other natural phenomena [38]. Brownian motions can be generated from a defined Hurst exponent and the data sets are sometimes referred to as fractional Brownian motion (abbreviated fBm). Fractional Brownian motion can be generated by a variety of methods, including spectral synthesis using either the Fourier transform or the wavelet transform. Here the spectral density is proportional to

$$\text{Spectral density } \alpha 1/f^{\beta}, \tag{1}$$

where $\beta = 2H + 1$ and $f$ is the frequency.

The fractal method is usually employed to extract information about stochastic behavior of time series. When the time series contains both a rapidly and a slowly varying trend, Hurst exponent is able to distinguish the following situations. For the long term trend, $H$ determines if the future of a time series trends is similar to its past. In this case the system is called persistent or positively correlated. For the short term memory, $H$ determines if the future of the time series tends to oppose its past. In this case, the system is called anti-persistent or negatively correlated. According to Darhos [34] $H > 0.5$ denotes a persistent process, i.e. the process exhibits a significant trend. For $H < 0.5$, the process behavior is anti-persistent, i.e. large positive values tend to be followed by large negative values. For the singular case $H = 0.5$, the process corresponds to uncorrelated Gaussian white noise. Despite the effectiveness of Hurst method in analyzing time series signals it suffers from the drawback that it is sensitive to the probe type and that calculations are highly time consuming [39].

### 4.3. Correlation dimension ($D_2$)

The correlation dimension is one measure of the fractal dimension of a chaotic system and is one of the most important measurements of chaotic behavior, because it quantifies the complexity of the chaotic attractor as well as providing a link to self-similar property of the fractal sets. Many authors [40–42] have utilized spatio-temporal chaos for to the analysis of two-dimensional patterns. As noted by Vazquez [33] and references therein, in extracting the correlation dimension, the time delay ($\tau$) and the embedding dimension ($d$) are very important parameters. If $\tau$ and $d$ are selected appropriately, the chaotic attractor is revealed. Thus, choice of the time delay is crucial at the very beginning of the reconstruction process. In a simple analogy, embedding a one-dimensional object (a line) in a two-dimensional space (a plane) confirms that it has a dimension of one, but embedding it in a three-dimensional space (a volume) reveals nothing further. The Recurrence Plot is a tool for determining $\tau$ and $d$ which will be outlined below. In the present work the $D_2$ calculation was realized by Visual Recurrence Analysis (VRA) v.4.9 software.

### 4.4. Recurrence plot (RP)

The recurrence plot can help determine the correct choices for both the embedding dimension and the embedding time delay [43,44]. According to Atay and Altintas [45], the two-dimensional *RP* can show intriguing patterns; however, they argue that many of these are an artifact of the way the embedding is done. If the embedding parameters are correctly chosen, only simple horizontal segments should be visible, and if the reconstruction actually represents the true dynamics, this can be directly observed in the *RP*. Non-horizontal lines on a recurrence plot indicate phase space vectors that are co-incidentally close but point in opposite directions, representing an incorrect choice of embedding dimension or time delay [45]. Although Atay and Altintas [45] only consider time series generated by smooth dynamical-systems, they assume that the time interval between measurements is sufficiently small to capture the smoothness of the trajectories. Hence, establishing a recurrence plot without non-horizontal patterns is the first step in the determination of the correct embedding parameters. However,

Kung-Sik and Howell [46] show recurrence plots for discrete time data in which diagonal lines are observed, and if these lines do not include isolated points, they state that the embedding dimension is determined correctly.

Thus, for the present rimming-flow analysis, a wide range of $\tau$ values were examined for each case, including but not limited to those suggested by *RP*; a similar approach was used by Vazquez [33] for bubbly flows. The ones presented below gave the most reasonable results, as determined by criteria such as the saturation of the correlation dimension.

## 5. Results and discussion

### 5.1. Results

The laser-signals and data points for each pattern are shown in Fig. 4; each time series is composed of $\geqslant$30,000 data points.

The Fourier spectral graphs are shown in Fig. 5. For the pool pattern (Fig. 4A) the characteristic frequency is zero and it is to presents secondary harmonics equally spaced at 0.2 and 0.4 Hz (Fig. 5A). The *FS* for the fingers pattern (Fig. 5B) shows significantly more noise than the *FS* for the other patterns (Fig. 5C–E) but the spectral trend is similar.

In order of obtain a pattern characterization, the correlation-dimension technique was applied (Fig. 6), in which the delay time was the $\tau$ value obtained when $D_2$ saturation is reached.

The recurrence maps (Fig. 7) show that in the pool pattern all points fall on the diagonal indicating that the pattern is very stable. Of course, this is because in this case the cylinder is stationary and no laser light dispersion is observed. The fingers and furrows are patterns with a similar behavior or structure, because many points occur on the diagonal. For the waterfall pattern, a different recurrence structure occurs, with a more random behavior, since more points occur away from the diagonal. A totally chaotic behavior is observed in the recurrence map for the smooth tooth pattern. This is clear because all points are dispersed and it is not possible to see any structure.

In order to better understand what happened when the patterns change, the Hurst exponent is calculated using the *FS* analysis and the results are plotted jointly with the $D_2$ values for each pattern (Fig. 8). It is interesting observe that while the $D_2$ have a zig-zag tendency, the $H$ values are always decreasing. The literature mention that the $H$ exponent indicates the time series behavior, which in this study represents the type or manner of the fluid motion. Strictly according to the definition (Section 4), the fingers pattern ($H > 0.5$) has 'long term memory' because the future of the time series trend is similar to its past. In contrast, the other patterns (furrows, waterfall and smooth tooth) have $H < 0.5$; the patterns are anti-persistent with large positive values followed by large negative values; from a geometric perspective, the anti-persistent series are more jagged than the $H > 0.5$ case, in which the series are smoother.

For the correlation dimension it is clear that in the pool pattern the series time is a horizontal line (Fig. 4A) and that one dimension is sufficient for cover or embed the pattern. When the correlation dimension increases from 1.08 to 2.26 it indicates that the fingers pattern is unstable with respect to pool pattern, and it is observed that points move away from the diagonal in the recurrence map (Fig. 7). Next, $D_2$ changes from 2.26 to 2.42; this rise in the $D_2$ value indicates that the furrows pattern is little more complex or random than the fingers pattern; this is corroborated by the recurrence maps (Fig. 7), in which is possible to see that in the furrows pattern, the liquid coating passes from stable to unstable states.

To seek an explanation of the previous pattern changes, consider the experimental forces in the thin liquid layer. At low speed rotation an internal liquid layer is added to cylinder (owing to the no slip condition) and the subsequent layers are pulled up. When the finger pattern is reached, liquid fingers are observed in the external liquid layer (the free surface) and they maintain a temporally stable shape, indicating that drag and surface tension forces have contributed to establish an equilibrium with the gravity force (see force diagram, Fig. 8). For this case the rotational effect is negligible. In the furrows pattern, the rotational velocity is greater than in the fingers case, and more liquid layers are pulled up the cylinder wall, but at the same time a greater mass of fluid is collected, and thus falls in the bottom of the cylinder. In this regime, the surface tension force not can maintain the fingers shape and the drag and gravity forces dominate the pattern; and again the rotational force is negligible.

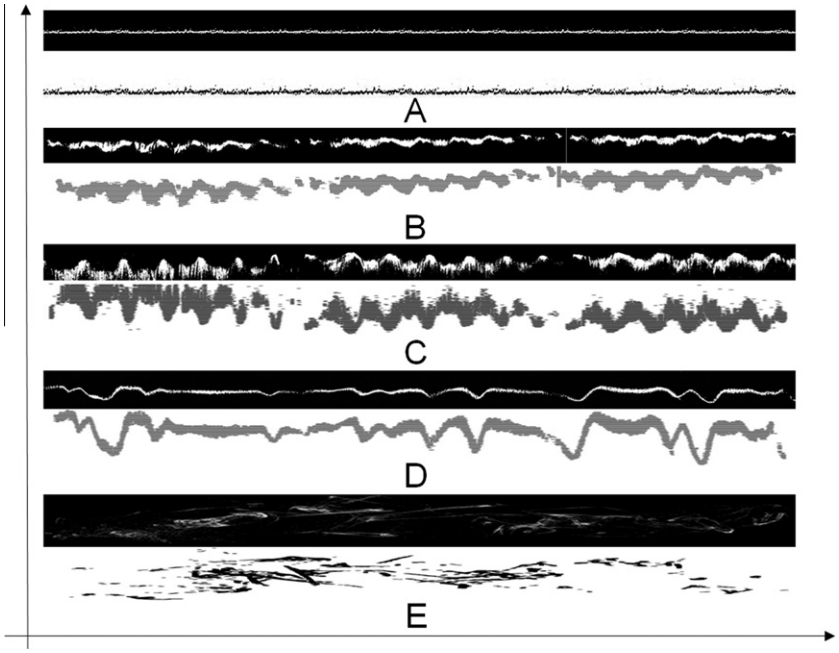


**Fig. 4.** Experimental binary-laser signals and time series for pool (A), fingers (B), furrows (C), waterfall (D), smooth tooth and (E) patterns.

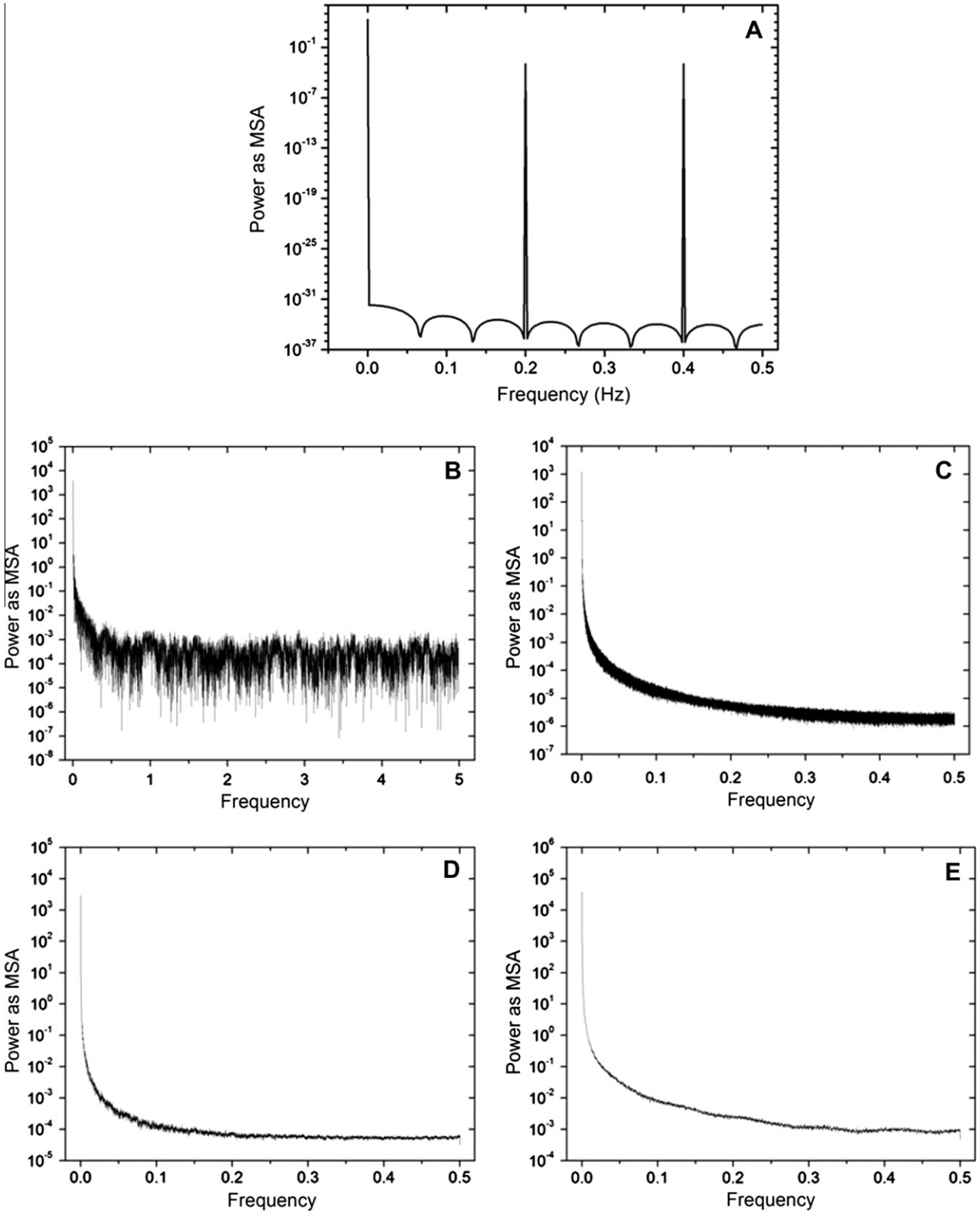


**Fig. 5.** Power spectrum for each pattern indicated in the (A–E).

As the rotation rate is further increased, $D_2$ falls from 2.42 to 2.15, which suggests that the waterfall pattern is more stable than the furrows pattern. This situation is not confirmed for the recurrence map (Fig. 7), because the waterfall recurrence map shows a more dispersed distribution, even though it is possible to observe a structure. In this respect, and considering the force diagram, more fluid is lifted up to the ascending wall of the cylinder, and consequently, the total gravitational force is increased and dominates the pattern. Therefore the surface tension force not is able to maintain the shape of the air–liquid free surface. This is

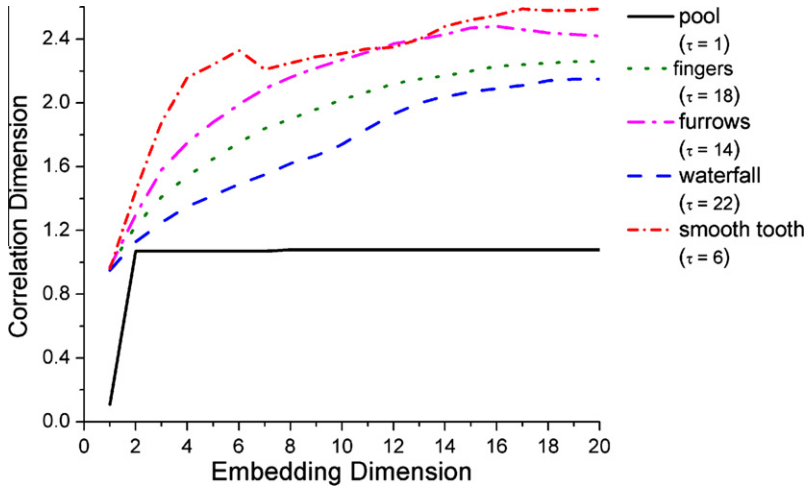


**Fig. 6.** Times delay and correlation dimension for pool ($\Omega = 0$), fingers, furrows, waterfall and smooth tooth patterns.

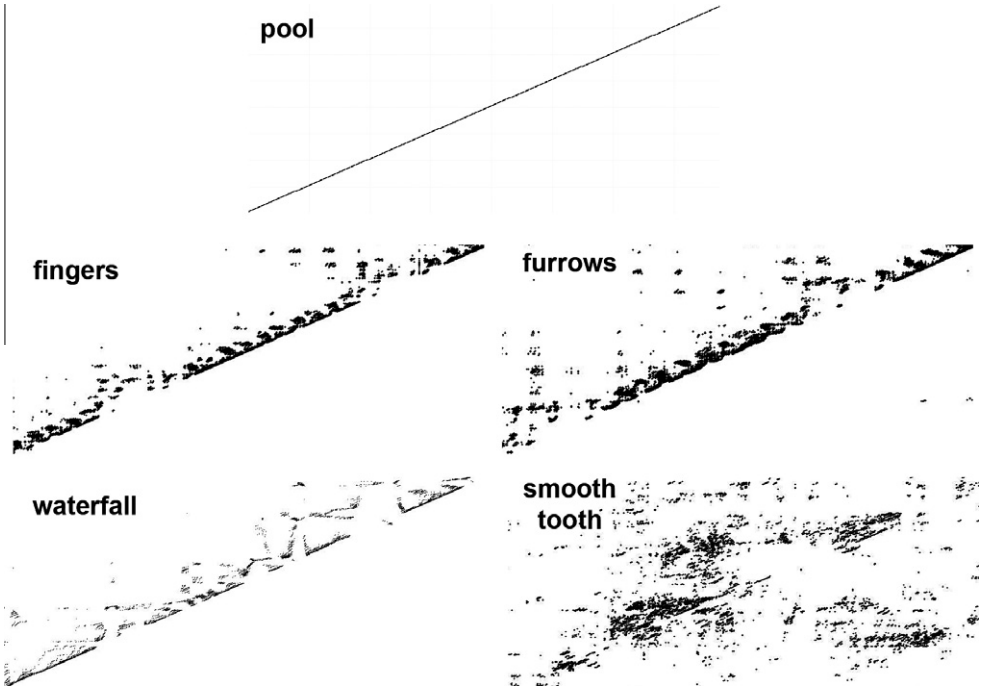


**Fig. 7.** Recurrence maps for the flow patterns.

observed when external liquid layers (near the free surface) slip over internal layers, generating the "waterfall" effect. The foregoing forces competition may be understand by dynamical-systems theory as if the liquid coat undergoes a self-organization.

Finally, the correlation dimension reaches a maximum value and in this sense the smooth tooth pattern is the most unstable or chaotic. This behavior is corroborated by the recurrence map (Fig. 7) in which many dispersed points break up the phase-space structure. In this regime, the rotational velocity is strong and carries away a great amount of liquid up the ascending wall. The drag and surface tension forces are unable to support the liquid in the wall, causing the liquid to fall to cylinder bottom, where the smooth tooth pattern is observed.

A summary of the dynamical-systems variables obtained in the study are shown in Table 1 (with the R-squared coefficient for the Hurst exponent added).

### 5.2. Discussion

#### 5.2.1. Flow patterns

The experimental work of Vallette et al. [7] corroborates the present the pattern-appearance order for low volume liquid fractions, but they do not mentioned the furrows pattern or the transient zones. This is justified because they were more focused on high Reynolds numbers, whereas for the present study the Reynolds range is low.

As noted in the Introduction, a minimum rotation speed has been proposed as a first parameter for flow-pattern characterization by Moffatt [23]; using this criterion, annular flow is reached at $St = 3.14$. In the present case, the Stokes number for annular flow is 5.77 at $\Omega = 5.2\ s^{-1}$; this is greater than that found by Moffatt [22]. It is possible that gravitational and viscous forces are not sufficient to select the patterns. The Reynolds number takes a higher

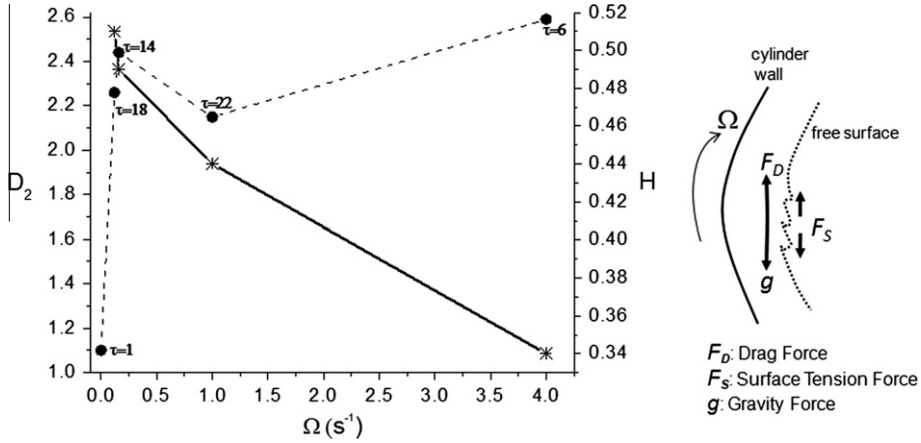


**Fig. 8.** Correlation dimension (circles) and Hurst exponent (asterisk) values for each flow pattern and forces diagram acting in rimming flow.

**Table 1**
Dynamical-systems (chaotic) parameters.

| Patterns | $\tau$ | $D_2$ | $H$ |
|---|---|---|---|
| Pool | 1 | 1.08 | Disable |
| Fingers | 18 | 2.26 | 0.51 ($R^2$ = 0.59) |
| Furrows | 14 | 2.42 | 0.49 ($R^2$ = 0.96) |
| Waterfall | 22 | 2.15 | 0.44 ($R^2$ = 0.88) |
| Smooth tooth | 6 | 2.59 | 0.34 ($R^2$ = 0.98) |

value (10.34) in the present study when annular flow is reached. In another attempt at characterize rimming flow patterns, a dimensionless number ($J$) was introduced by Preziosi and Joseph [24]. They indicate that if $J > 4$ the annular pattern could occur. In the present case $J = 39$ (for $\Omega = 5.2\ s^{-1}$) which is at least consistent with Preziosi and Joshep's criterion because an annular flow was observed in the present experiment. The large disparity in values of $J$ for annular flow between Preziosi and Joseph [24] and ourselves suggests that inertia and surface tension alone are not the sole pattern-selection forces. Many factors including rotational inertia, surface, tension, gravitational and viscous forces may be relevant as well as geometric parameters such as the coating thickness (filling fraction), and cylinder radius.

*5.2.2. The spectral and chaotic analysis*

After the above time series data analysis, we believe that the *FS* technique not is a good tool to indicate the pattern transitions. This is because the spectral trend for fingers, furrows, waterfall and smooth tooth patterns is very similar and not is possible distinguish any change in the frequency; however this trend resembles fractal behavior, so that the *FS* can suggests an self-similarity tendency.

The flow transitions are better represented by the recurrence maps. These maps can reveal the new liquid structures even if the rotating velocity changes are minor. There is an interesting contrast with the Hurst exponent. As detailed above, the Hurst parameter established two different phenomena for the fingers and furrows patterns, but the recurrence maps suggested that these patterns are correlated. We believe that in this sense the Hurst classification is confusing for values in the neighborhood of 0.5. The literature indicate that values $H \approx 0.5$ white noise behavior is observed [35], or possibly that if the series time are very short (<3000 points), the Hurst accuracy not is reliable. However, in the present work, the time series has approximately 30,000 data points.

With respect to the Hurst exponent trend, the negative slope observed may be valid if we only consider flow patterns greater than 0.5 such as the waterfall and smooth tooth.

Comparing the $D_2$ results in Fig. 8 with the phase diagram for the rimming flow (Fig. 3) it is possible see that when the fluid patterns (fingers and waterfall) are localized on the rotating ascending wall, the correlation dimension values show more stable regimes whereas for the regimes with greater random fluctuations (the furrows and smooth tooth patterns) are located on the cylinder bottom. It is true that the time series for the furrows and smooth tooth patterns have irregular or higher amplitude saw shapes, which have an important influence on the $D_2$ calculation. This calculation reports that these patterns show characteristics of metastable systems. On the contrary, the smoothness of the fingers and waterfall time series indicate that the free-surface evolution is not affected by small changes in the rotational velocity, and therefore shows characteristics of stable systems.

Summarizing the discussion above and taking account our experimental observations, we suggest that in the stable systems, small changes in $\Omega$ do not significantly modify the force competition in the free surface, while for meta-stable systems, small changes in the rotational speed have an important influence on the force competition.

## 6. Conclusions

Rimming flow has been observed at very low volume fractions, quantitative data obtained by a novel technique, and an assessment has been made of the efficacy of various dynamical-systems analysis for the characterization of the patterns.

The fluid patterns we report are in agreement with those of previous authors, although the fingers and furrows patterns not are generally reported.

The results indicate that the laser-light technique is able to obtain time series data from each pattern. The analysis for these time series show that the *FS* method not can characterize the patterns but can indicate the noise level in the signals and a fractal trend in the time series.

With respect to dynamical-systems (chaotic) analyzes, the Hurst exponent is a good tool for determining when a new pattern appears, but not can detect clearly if this pattern is more chaotic or stable that the previous pattern.

The recurrence plots can be a reliable option for demonstrating the flow transitions and the system stability (qualitatively), and are a good complement to the correlation dimension.

Finally we conclude that the correlation dimension is an adequate tool for characterizing rimming-flow fluid patterns. Using the correlation dimension, it is possible to observe pattern transi-

tions, to determine if the pattern is stable or chaotic, and to understand the force competition in the free surface.

## References


[1] J. Ashmore, A.E. Hosoi, H.A. Stone, The effect of surface tension on rimming flows in a partially filled rotating cylinder, J. Fluid Mech. 479 (2003) 65–98.
[2] E.S. Benilov, S.B. O'Brien, Inertial instability of a liquid film inside a rotating horizontal cylinder, Phys. Fluids 17 (2005) 052106.
[3] T.D. Karapantsios, N.A. Tsochatzidis, A.J. Karabelas, Liquid distribution in horizontal axially rotated packed beds, Chem. Eng. Sci. 48 (8) (1993) 1427–1436.
[4] H. Benkreira, R.I. Pate, M.F. Edwards, W.L. Wilkinson, Classification and analysis of coatings flows, J. Non-Newtonian Fluid. Mech. 54 (1994) 437–447.
[5] B.I. Wilhelmsson, J.F. McKibben, S.G. Stenström, C.K. Aidun, Condensate flow inside paper dryer cylinders, J. Pulp Pap. Sci. 21 (1995) J1.
[6] S. Sandadi, P. Pandey, R. Turton, In-situ near real-time acquisition of particle motion in a rotating pan coating equipment using imaging techniques, Chem. Eng. Sci. 59 (24) (2004) 5807–5817.
[7] D.P. Vallette, G. Jacobs, J.P. Gollub, Oscillations and spatiotemporal chaos of one-dimensional fluid fronts, Phys. Rev. E 55 (4) (1997) 4274–4287.
[8] P.J. Chen, Y.T. Tsai, T.J. Liu, Low volume fraction rimming flow a rotating horizontal cylinder, Phys. Fluids 19 (2007) 128107-1–128107-4.
[9] P.L. Evans, L.W. Schwartz, R.V. Roy, Three-dimensional solutions for coating flow on a rotating horizontal cylinder: Theory and experiments, Phys Fluids 17 (8) (2005) 072102-1–072102-20.
[10] R.E. Johnson, Steady-state coating flows inside a rotating horizontal cylinder, J. Fluid Mech. 190 (1998) 321–342.
[11] R.E. Johnson, in: Engineering Science, Fluid Dynamics: A Symposium to Honor Wu T.Y, World Scientific Singapore, 1990.
[12] F. Melo, Localized states in a film-dragging experiments, Phys. Rev. E 48 (1993) 2704–2712.
[13] M. Tirumkudulu, A. Acrivos, Coating flows within a rotating horizontal cylinder: lubrication analysis, numerical computations, and experimental measurements, Phys. Fluids 13 (2001) 4–18.
[14] G.R. Shrager, M.N. Shtokolova, V.A. Yakutenok, Formation of the free surface of a viscous fluid volume inside a rotating horizontal cylinder, Fluid Dyn. 44 (2009) 322–327.
[15] G. Bohme, G. Pokriefke, A. Muller, Viscous flow phenomena in a partially filled rotor-stator system, Arch. Appl. Mech. 75 (2006) 619–634.
[16] R.T. Balmer, The hygrocyst -a stability phenomenon in continuum mechanics, Nature 227 (1970) 600–601.
[17] M.J. Karweit, S. Corrsin, Observations of cellular patterns in a partly filled horizontal cylinder, Phys. Fluids 18 (1975) 111–112.
[18] J.P. Kovac, R.T. Balmer, Experimental studies of external hygrocysts, J. Fluids Eng. 102 (1980) 226–230.
[19] R. Chicharro, Patterns Developed in Rotating Flows with Free Surface, Master thesis, Mexico City, FC-UNAM, 1995.
[20] S.T. Thoroddsen, L. Mahadevan, Experimental stuffy of coating flows in a partially-filled horizontal rotating cylinder, Exps. Fluids 23 (1997) 1–13.
[21] O.A.M. Boote, P.J. Thomas, Effects of granular additives on transition boundaries between flow states of rimming flows, Phys. Fluids 11 (8) (1999) 2020–2029.
[22] M. Tirumkudulu, A. Tripathi, A. Acrivos, Particle segregation in monodisperse sheared suspensions, Phys. Fluids 11 (1999) 507–510.
[23] H.K. Moffatt, Behaviour of a viscous of outer surface of a rotating cylinder, J. Mech. 16 (1977) 651–673.
[24] L. Preziosi, D.D. Joseph, The run-off condition for coating and rimming flows, J. Fluid Mech. 187 (1988) 99–113.
[25] S. Fomin, Three regimes of non-newtonian rimming flow, J. Fluid Eng. 128 (2006) 107–112.
[26] R. Clift, J.R. Grace, M.E. Weber, Bubbles, Drops and Particles, Academic Press, London, 1978.
[27] T.J. Lin, R.C. Juang, Y.C. Chen, C.C. Chen, Predictions of flow transitions in a bubble column by chaotic time series analysis of pressure fluctuations signals, Chem. Eng. Sci. 56 (3) (2001) 1057–1065.
[28] J. van der Schaaf, J.C. Schouten, F. Johnsson, C.M. van den Bleek, Non-intrusive determination of bubble and slug length scales in fluid beds by decomposition of the power spectral density of pressure time series, Int. J. Multiphase Flow 28 (2002) 865–880.
[29] R. Mosdorf, M. Shoji, Chaos in bubbling-nonlinear analysis and modeling, Chem. Eng. Sci. 58 (2003) 3837–3846.
[30] V.P. Chilekar, M.J.F. Warnier, J. van der Schaaf, B.F.M. Kuster, K.C. Schouten, J.R. van Ommen, Bubble size estimation in slurry bubble columns from pressure fluctuations, AIChE J. 51 (2005) 1924–1937.
[31] L.S. Fan, Y. Kang, D. Neogi, M. Yashida, Fractal analysis of fluidized particle behavior in liquid–solid fluidized beds, AIChE 39 (1993) 513–517.
[32] P. Kolodner, S. Slimani, N. Aubry, R. Lima, Characterization of dispersive chaos and related states of binary-fluid convection, Physica D 85 (1995) 165–224.
[33] A. Vazquez, R. Manasseh, R.M. Sánchez, G. Metcalfe, Experimental comparison between acoustic and pressure signals from a bubbling flow, Chem. Eng. Sci. 63 (2008) 5860–5869.
[34] M.A. Latifi, A. Naderifar, N. Midoux, A. Le Mehaute, Fractal behavior of local liquid–solid mass transfer fluctuation at the wall of a trickle bed reactor, Chem. Eng. Sci. 49 (1994) 3823–3829.
[35] J.J. Drahos, F. Bradka, M. Puncochar, Fractal behavior of pressure fluctuations in bubble column, Chem. Eng. Sci. 47 (1992) 4069–4075.
[36] G.W. Baxter, R. Leone, R.P. Beheringer, Experimental test of time scales in flowing sand, Europhys. Lett. 21 (5) (1993) 569–574.
[37] J. Andrade, C. Treviño, A. Medina, Experimental evidence of density fluctuations in two-dimensional bins, Phys. Lett. A 223 (1996) 105–110.
[38] C.I. Briens, I.A. Briens, J. Hay, C. Hudson, A. Margaritis, Hurst's analysis to detect minimum fluidization and gas mal distribution in fluidized beds, AIChE 43 (1997) 1904–1911.
[39] S. Boccaletti, J. Bragard, F.T. Arecchi, Controlling and synchronizing space time chaos, Phys. Rev. E 59 (6) (1999) 6574–6578.
[40] J. Bragard, S. Bocaletti, C. Mendoza, H. Hentschel, H. Mancini, Synchronization of spatially extended chaotic systems in the presence of asymmetric coupling, Phys. Rev. E 70 (3) (2004) 036219.
[41] M.B. Kennel, R. Brown, H.D.I. Abarbanel, Determining embedding dimension for phase-space reconstruction using a geometrical construction, Phys. Rev. A 45 (1992) 3403–3411.
[42] H.D.I. Abarbanel, Analysis of Observed Chaotic Data, Springer, New York, 1996.
[43] J.P. Eckman, S.O. Kamphorst, D. Ruelle, Recurrence plots of dynamical systems, Europhys. Lett. 4 (1987) 973–977.
[44] G.B. Mindlin, H.G. Solari, M.A. Natiello, R. Gilmore, X.-J. Hou, Topological analysis of chaotic time series data from the Belousov–Zhabotinskii reaction, Nonlinear Sci. 1 (1991) 147–173.
[45] F.M. Atay, Y. Altintas, Recovering smooth dynamics from time series with aid of recurrence plots, Phys. Rev. E 59 (1999) 6593–6598.
[46] C. Kung-Sik, T. Howell, Chaos: A Statistical Perspective, Springer, 2001.